ORIGINAL ARTICLE

lajss.org
Latin American Journal of Solids and Structures

www.lajss.org

# Experimental Study on The Effect of Fracture Strain on the Fragmentation Effect of PELE

**Yuheng Liu[a], Lizhi Xu[b]*, Heling Zheng[a], Meng Xu[a], Wenzheng Lv[b], Zhonghua Du[b]**

[a]School of Equipment Engineering, Shenyang Ligong University, Shenyang,110158, China. E-mail: 1223674864@qq.com, 316580379@qq.com, xu18137500689@163.com
[b]School of Mechanical Engineering, Nanjing University of Science and Technology, Nanjing,210094, China. E-mail: 13770318390@163.com, lwz20210407@njust.edu.cn, duzhonghua@yahoo.com.cn

*Corresponding author

https://doi.org/10.1590/1679-78257496

## Abstract

The fragmentation effect of PELE refers to the fragmentation of the jacket after PELE penetrates the metal target plate. Three sets of 30CrMnSiA tensile samples with different hardness were pulled to obtain the corresponding maximum principal tensile stress and fracture strain of the material. It was found that the greater the hardness, the smaller the fracture strain, and the more easily to shear failure; Then, PELE penetration metal thin target fragment recovery test was carried out. It was found that only HRC50 jacket had compression shear and other brittle material damage characteristics and produced ideal fragmentation effect during penetration; The results show that the greater the target velocity is, the greater the critical value of its own material breaking is. When its own breaking strain is less than the critical value, the jacket can play a fragmentation effect; For PELE penetrator with the same material performance that meet the crushing conditions, the greater the impact velocity, the more the number of jacket fragments and the larger the distribution radius of fragments.

## Keywords

PELE (the Penetrator with Lateral Efficiency); fragmentation effect; Critical fracture strain; Fragment morphology

## Graphical Abstract

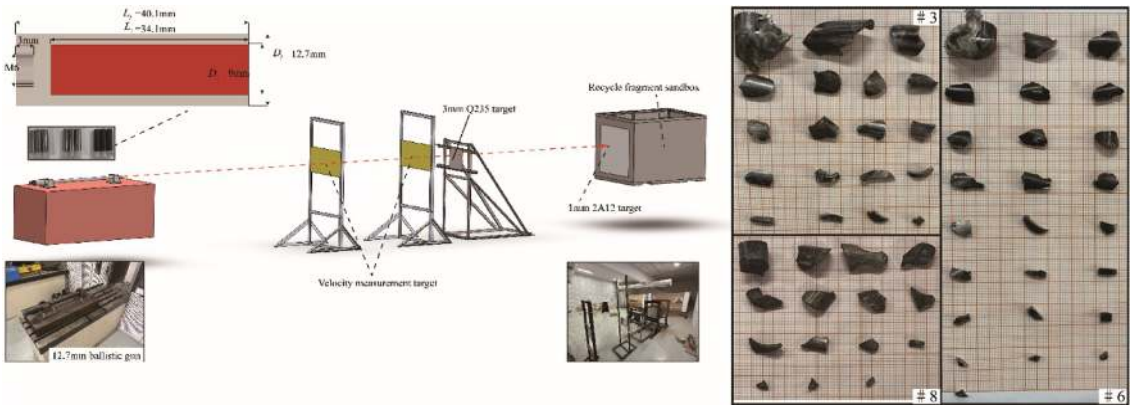


Received February 04, 2023. In revised form February 13, 2023. Accepted June 14, 2023. Available online June 21, 2023.
https://doi.org/10.1590/1679-78257496

Latin American Journal of Solids and Structures. ISSN 1679-7825. Copyright © 2023. This is an Open Access article distributed under the terms of the Creative Commons Attribution License, which permits unrestricted use, distribution, and reproduction in any medium, provided the original work is properly cited.

## 1 INTRODUCTION

Penetrator with Enhanced Lateral Effects (PELE) can produce a large number of fragments (called PELE fragmentation effect) after penetrating a finite thickness metal target , which can effectively damage the target behind the target. Therefore, the fragmentation effect of PELE has important military application value in weapons and ammunition such as anti-armed helicopters, armored vehicles, ships and so on, and its scientific problems have been widely concerned by scholars at home and abroad. The concept of Penetrator with Enhanced Lateral Effects (PELE) was first published at the 24th International Ballistics Conference , and scholars at home and abroad have carried out research on the theoretical model and influence law of PELE fragmentation. In the research on the impact of PELE jacket material properties, Zhu et al. (2010) selected PELE jacket material as ordinary tungsten alloy and brittle tungsten alloy with different tensile and compressive strength, It was found that with the increase of the tension-compression strength ratio, the number of fragments and the distribution radius decreased significantly. Chen (2014) studied the impact of the tensile fracture strain of tungsten alloy jacket on the PELE fragmentation effect through numerical simulation. The results showed that the radial velocity and the number of fragments gradually decreased with the increase of the tensile fracture strain (within the range of 0.05~0.30). Fan (2016) analyzed the impact of the wave velocity of the jacket material on the PELE fragmentation effect, found that the radial velocity of the fragments decreased with the increase of the density of the jacket material, and determined that the wave velocity of the jacket material was not the main influencing factor of the fragmentation effect. Then scholars analyzed the fracture and fracture theory of PELE jacket, and the Liang combined numerical simulation and experiment to study the penetration of PELE into metal target, and deduced the damage and fracture equation of PELE jacket; The parameters of the jacket expansion and fracture process are calculated through a case study of jacket fracture, and the relationship between the impact velocity of the penetrator and the jacket fracture is analyzed. Based on the impact dynamics and material fracture theory, Chun et al. (2019) established a mechanical model of PELE penetrating the metal target plate by comprehensively considering the shock wave propagation, the elastoplastic compression deformation of the filling, the radial expansion deformation and fragmentation of the jacket, and analyzed the impact compression of the filling, the radial stress distribution in the filling, the stress on the jacket, the fragmentation of the jacket and the distribution of the fragments in the process of PELE acting on the metal target plate, revealing the mechanical mechanism of PELE acting on the metal target plate, The whole change process of PELE during penetrating the target plate is described theoretically, and the fragment distribution rule of PELE after penetrating the target plate is obtained, and the fracture mode of PELE jacket is clarified from macro and micro scales. From the above research basis, it can be found that the research on the impact of the PELE fragmentation effect lacks the research on the impact of the same jacket material, different strength and fracture strain on the jacket crushing. In this paper, 30CrMnSiA is used as the jacket material of PELE. By changing the degree of heat treatment of the jacket and then changing the fracture strain, the influence rule of the jacket fracture strain on the PELE fragmentation effect is explored. The measurement of the strength of the fragmentation effect is reflected in the fragment distribution radius, quantity and size distribution.

## 2 DYNAMICS PERFORMANCE TEST OF 30CRMNSIA WITH DIFFERENT HARDNESS

### 2.1 Tensile test

According to the requirements of the national standard GB/T 228.1-2010, the size and shape of the tensile pattern are designed, and the steel blanks are heat treated to different degrees to obtain three kinds of steel with different hardness and processed into tensile samples, the physical drawing and design dimensions are shown in Figure 1. Conduct quasi-static tensile test of materials, and ensure that all tensile samples are stretched at the same strain rate by setting the tensile rate of universal material testing machine. Set the tensile rate to 50mm/min during the test, and the corresponding strain rate is $1\times10^{-2}s^{-1}$. Nine tensile tests were conducted at total, and three tests were conducted for tensile samples with the same hardness.

Two sets of test data, axial tensile force and displacement, are finally obtained through the universal material testing machine. They are transformed into the real stress strain of the material through their relationship with the initial diameter and length of the sample and the assumption of incompressibility of the material. The calculated parameters of three groups of tensile samples are shown in Table 1.

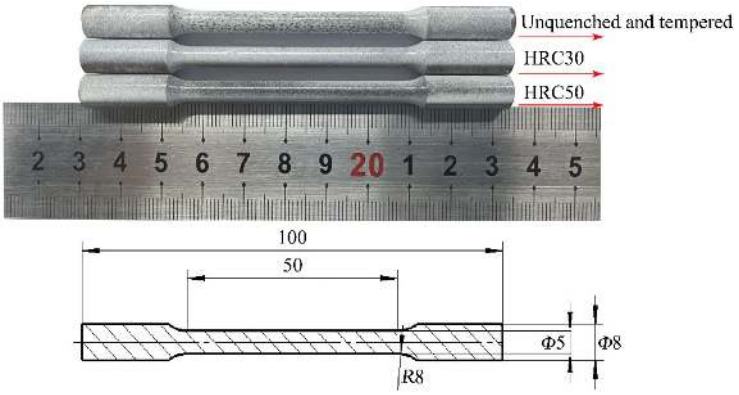


**Fig.1** Dimension and appearance of tensile sample with different heat treatment degrees

**Table 1** Fracture parameters of tensile samples with different hardness

| | Sample No | Fracture strain/$\varepsilon_f$ | Average fracture strain | Maximum principal tensile stress $\sigma$/GPa |
|---|---|---|---|---|
| Unquenched and tempered | #1-1 | 0.0799 | 0.0747 | 1.018 |
| | #1-2 | 0.0651 | | 1.013 |
| | #1-3 | 0.079 | | 1.065 |
| HRC30 | #2-1 | 0.0329 | 0.0372 | 1.204 |
| | #2-2 | 0.0369 | | 1.217 |
| | #2-3 | 0.0417 | | 1.200 |
| HRC50 | #3-1 | 0.0256 | 0.0267 | 1.504 |
| | #3-2 | 0.0217 | | 1.510 |
| | #3-3 | 0.0327 | | 1.548 |

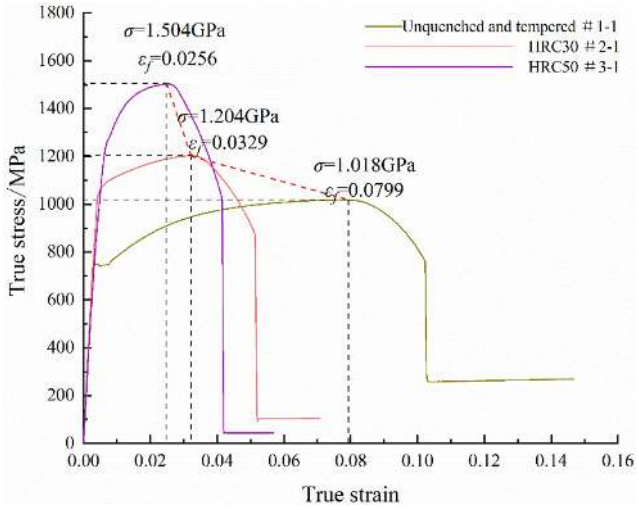


**Fig.2** True stress true strain curves of tensile samples with different hardness

In order to explore the change of fracture parameters of tensile samples when the hardness increases, the values in each group have little difference, select one test result from each group of samples for comparison, and the change trend is shown in Figure 2. From the data in Table 1 and the curve change trend in Figure 2, it can be seen that under the same strain rate, with the increase of the hardness of the tensile sample, the fracture strain of the tensile sample $\varepsilon_f$ decreases, the maximum tensile principal stress $\sigma$ enlarge.

## 2.2 Fracture morphology analysis of sample

The section morphology of three groups of tensile test sample with different hardness after tensile test is shown in Figure 3. It can be observed that the fracture morphology of the unquenched and tempered sample is similar to the HRC30 sample. The local area of the fracture has necking, and the fracture has large plastic deformation. Deformation is cup-shaped, which is a typical ductile fracture. The degree of necking decreases with the increase of material hardness; When the hardness of the sample increases to HRC50, the necking degree of test samples #3-1 and 3-2 continues to weaken, but the fracture surface of test sample # 3-3 not occurs obvious necking, and the fracture surface and the axial direction of the sample show a 45 ° shear fracture, which is a typical brittle fracture .

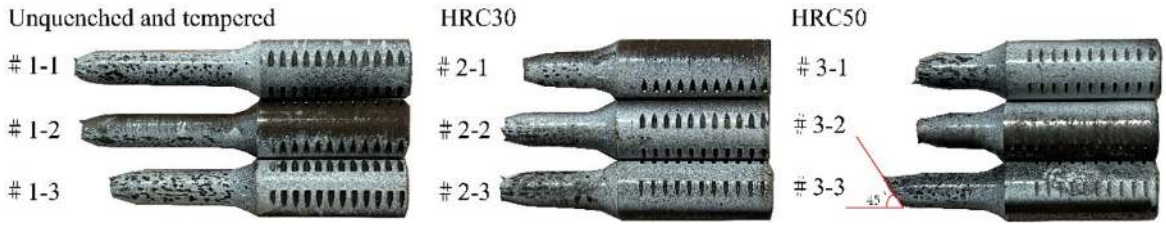


**Fig.3** Different tensile samples after fracture

By observing the fracture section morphology of unquenched and tempered and HRC30 samples, the fracture section can be divided into fiber area, radiation area and shear lip. Taking # 1-1 in Figure 4 as an example, the central circle area is the fiber area, which is the initial area of fracture, and the surface is rough fiber; From the fiber circle spread to the all around, the divergent radiation area is formed. When the crackle extends to the fiber area, the crackle growth speed slows down, forming serrations; The bright area of the fracture edge is the shear lip, which surface is smooth, and the slope of the shear lip is 45 ° to the direction of tensile stress. The fracture mode of the tensile samples with these two kinds of hardness is typical ductile fracture; Comparing the fracture sections of two different hardness samples, the higher the hardness is, the smaller the fracture strain is, the larger the proportion of radiation area in the section is, the wider the serrated crack is, and the smaller the proportion of fiber area and shear lip is; When observing the fracture sections of HRC50 tensile samples, the radiation area of section # 3-1 and section # 3-2 disappeared, only the fiber area and the shear lip, and the fiber area section was flat compared with the first two hardness; The fracture section of sample # 3-3 is 45° to the axial direction of the sample, which is a typical brittle fracture.

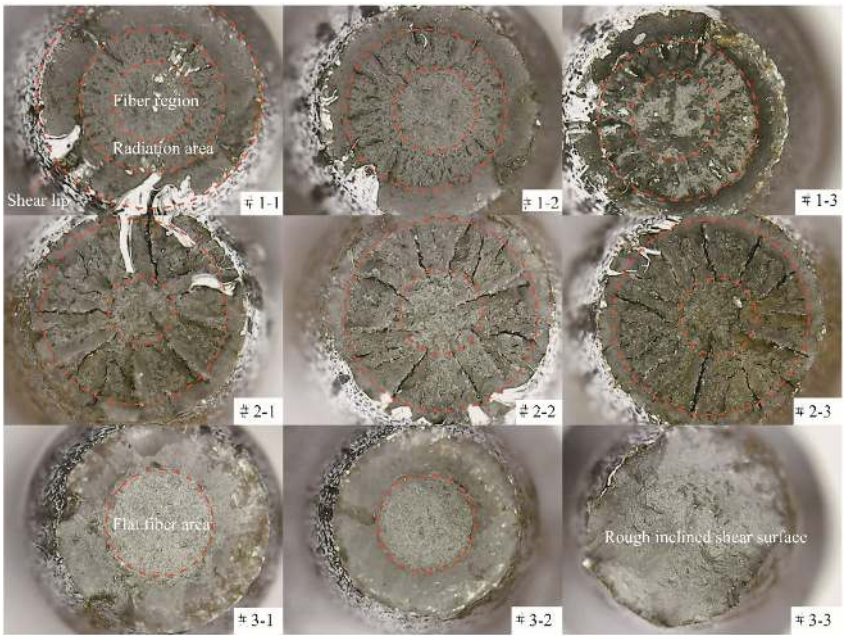


**Fig. 4** Fracture section morphology of tensile samples with different hardness

## 3 PELE PENETRATION THIN STEEL PLATE FRAGMENT RECOVERY TEST

### 3.1 Ballistic test

The test uses a 12.7mm ballistic gun as the launch platform. The Q235 main target is 3 meters perpendicular to the muzzle, and the size of the main target is 300mm × 300mm × 3mm. A fragment collection sandbox with 2024AL aftereffect target is arranged at 710mm behind the main target in parallel to collect fragments generated by the fragmentation of PELE penetrator through the target. The aftereffect target size is 450mm × 450mm × 1mm, an on-off target is arranged in front of the main target to measure the impact velocity of PELE penetrator. PELE penetrator consists of 30CrMnSiA jacket, 1060AL filling and nylon bottom bracket. The jacket $L_1$ is 40mm long, the diameter $D_1$ is 12.7mm, the filling $L_2$ is 34.1mm long, and the diameter $D_2$ is 9mm; The jacket and bottom bracket are connected by M6 thread. The mass of jacket, filling and bottom bracket are about 21g, 6g and 1g respectively. The ballistic test layout and penetrator size parameters are shown in Figure 5.

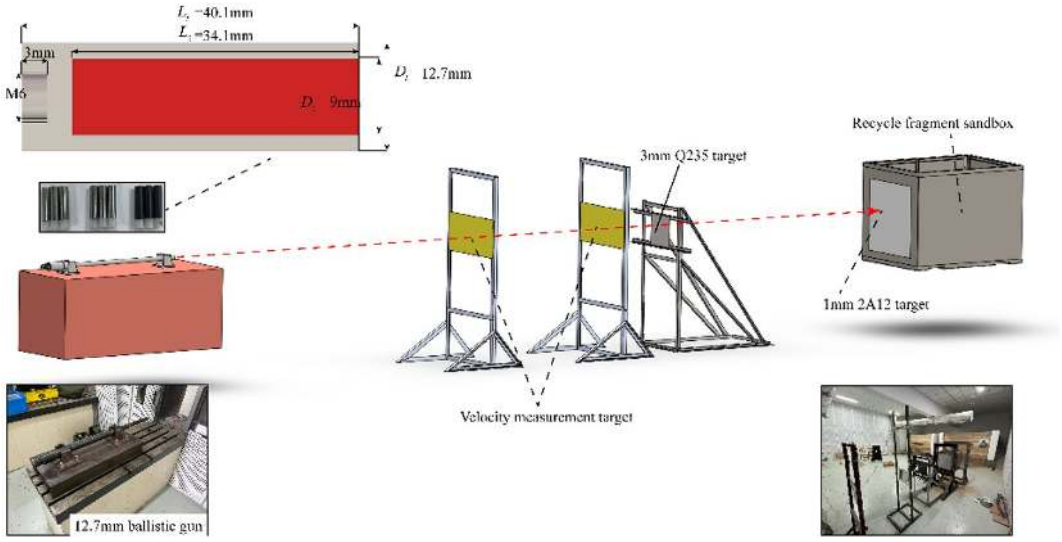


**Fig.5** Ballistic test

In order to explore the effect of fracture strain on jacket crushing, the jacket hardness corresponds to the three different tensile samples mentioned above. The hardness, impact velocity, target material and thickness of target in the test are shown in Table 2.

**Table 2** jacket hardness, impact velocity, target material and thickness in the test

| Sample No | Jacket hardness/HRC | Target velocity/(m/s) | Target material | Thinness of target/mm |
|---|---|---|---|---|
| #1 | Unquenched and tempered | Unmeasured | Q235 | 3 |
| #2 | HRC50 | 733 | Q235 | 3 |
| #3 | HRC50 | 892 | Q235 | 3 |
| #4 | HRC30 | 804.5 | Q235 | 3 |
| #5 | HRC50 | 886.2 | Q235 | 3 |
| #6 | HRC50 | 937.2 | Q235 | 3 |
| #7 | HRC30 | 740 | Q235 | 3 |
| #8 | HRC50 | 787.5 | Q235 | 3 |

### 3.2 Target opening size analysis

In order to explore the influence of PELE penetrator with different fracture strain on the opening size of thin target, all the opening sizes on Q235 main target were measured. If the opening shape is approximately circular, it shall be defined according to the circle radius *R*; The approximate ellipse shape is defined by the 1/2 power of the product of the major axis and the minor axis of the ellipse. The measured target opening size and the front and back surface morphology of the through-hole are shown in Figure 6.

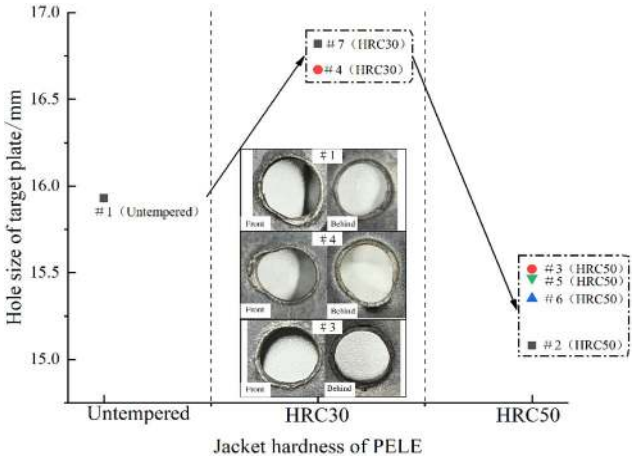


**Fig.6** Hole size of PELE penetration with different hardness for target and hole morphology of target

According to the hole size measured in Figure 6, if the hole size of HRC50 jacket is smaller than that of Unquenched and tempered and HRC30, the minimum size is 15.08mm and the maximum size is 15.52mm; The hole size of the jacket without quenching and tempering is 15.93mm, and the hole size of the HRC30 is 16.67mm and 16.82mm. Observe the shape of PELE penetrator after passing the target as shown in the figure 7. In test # 1 (Unquenched and tempered), PELE penetrator did not produce fragments. The jacket of the penetrator was squeezed radially by the filling under high-speed impact, the surface expanded outward, and the front end of the jacket was compressed backward after being impacted by the target, finally forming a "horn shape"; In test # 4 (HRC30), the degree of head damage of PELE penetrator after penetrating the target increased compared with that of # 1. The front 1/3 of PELE jacket was bent and deformed without fracture, while the remaining 2/3 of the front end could be bent and fractured, and the jacket along the axial direction of the penetrator was almost not deformed; The hardness increases, the jacket strength increases, the deformation degree decreases, the opening size decreases, and the opening size of the target plate should decrease on the premise that the whole is not broken, but the opening size in Figure 6 does increase, which is due to the incorrect angle of the target from the perspective of the opening shape. The reason for the fracture of the head jacket is due to the complex situation of the interaction between the filling and the target, which is not necessarily related to the compression shear.




**Fig.7** PELE penetration behind target shape

### 3.3 HRC50 jacket fragment mass and size statistics

Through the comparison above, it is known that PELE projectile play a breaking effect when the jacket hardness reaches HRC50 in the range of target speed. The shape and size of fragments collected in three groups of HRC50 tests are shown in figure 8. The fragments can be divided into head fragments, middle fragments and bottom fragments according to the shape and size of fragments. Head fragments are mostly triangular or rectangular in shape, triangular fragments have 0.5mm at both right-angled edges and 0.5mm in length for rectangular fragments. × 1mm; Middle and bottom fragments are irregular in shape and about 1mm × 1mm in size. The collected fragments are weighed and the mass fragments of each fragment are weighed (excluding the unbroken bottom) as shown in Table 3.

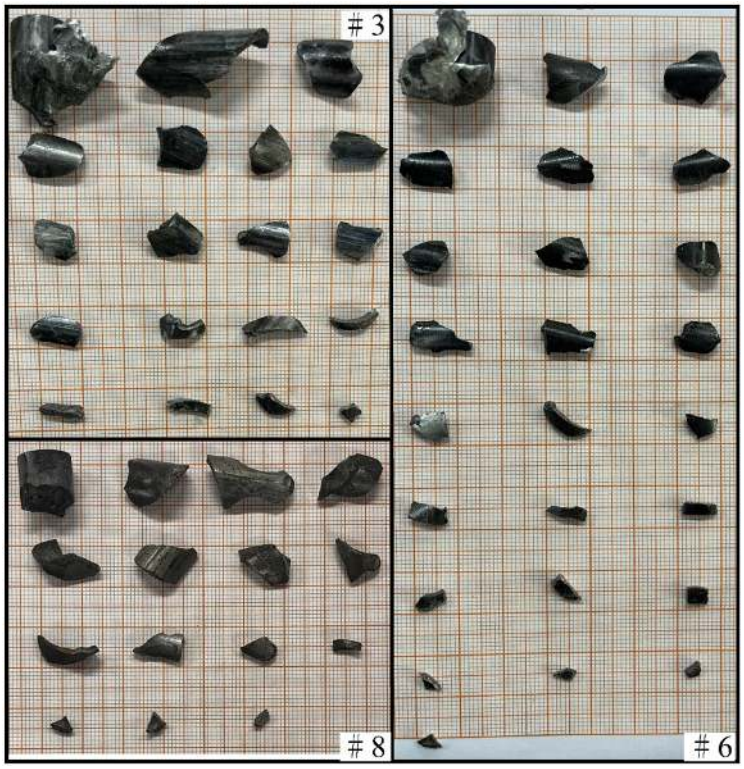


**Fig.8** Recovery of fragments of PELE jacket

**Table 3** PELE jacket fragment quality and number

| **Test No** | **#3** | | | | | |
|---|---|---|---|---|---|---|
| Fragment mass/g | 4.63 | 1.85 | 1.38 | 1.13 | 1.05 | 0.97 |
| | 0.78 | 0.77 | 0.88 | 0.68 | 0.41 | 0.48 |
| | 0.32 | 0.16 | 0.78 | 0.38 | 0.30 | 0.78 |
| Fragment quantity /g | 18 | | | | | |
| Test No | #6 | | | | | |
| Fragment mass/g | 1.49 | 1.42 | 0.94 | 0.93 | 0.87 | 0.85 |
| | 0.86 | 0.80 | 0.72 | 0.71 | 0.59 | 0.44 |
| | 0.44 | 0.33 | 0.25 | 0.24 | 0.21 | 0.26 |
| | 0.23 | 0.12 | 0.01 | 0.01 | 0.01 | 0.28 |
| Fragment quantity /g | 24 | | | | | |
| Test No | #8 | | | | | |
| Fragment mass/g | 2.07 | 2.16 | 1.83 | 1.48 | 1.24 | 1.11 |
| | 1.00 | 0.77 | 0.68 | 0.39 | 0.18 | 0.10 |
| | 0.09 | | | | | |
| Fragment quantity /g | 13 | | | | | |

The percentage of fragments with different quality in each group is shown in Figure 9. It is known that the fragments with the best fragmentation effect in #6 have the largest proportion in the range of 0.01-0.5g.

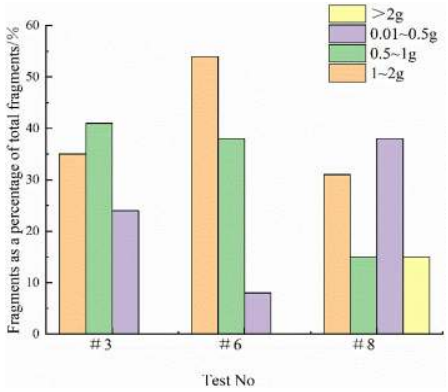


**Fig.9** Percentage of fragments with different quality in each group

Relating the PELE penetration targeting velocity to the number of fragments, it can be found that under the same fracture strain jacket PELE, the higher the targeting velocity, the more fragments will be produced behind the target. The targeting velocity is 787.5m/s, and the number of fragments produced is 13; The targeting velocity is 892m/s. the number of fragments produced is 18; The targeting velocity is 937.2m/s, and the number of fragments produced is 24; With the increase of the target velocity and the impact pressure on the filling, more stress and strain rate will be produced on the inner wall of the jacket, which will lead to more adequate fragmentation and more fragments in the head and middle.

### 3.4 Fragment macroscopic morphology analysis

Select test # 6 with a large number of fragments to observe the macro morphology of various fragments and analyze their formation mechanism. The jacket only breaks in the axial and radial directions, without damage in the thickness direction; The triangular head fragment is shown in Figure 10 (*a*) (*b*) , which is small in size and is approximately an isosceles right-angled triangle with an inclined edge of 5mm long. There are damage marks on the inclined edge caused by impact on the target, so it can be determined that such fragments are the most front end of the jacket; By measuring the thickness of the fragments, it is found that no obvious plastic strain occurs in the thickness direction of each part of the fragments, because the quenched and tempered steel is a brittle material, and the shell will break when it produces a small radial strain.

For the middle fragment (*c*) (*d*) (*e*) and bottom fragment (*f*), in the impact direction, because the pressure along the axial direction of the penetrator gradually decreases, the radial expansion velocity of the jacket slows down, the radial width of the fragment increases, and the section directions on both sides are more parallel to the axis, which is tensile fracture; The angle between the two smooth fracture surfaces at the impact end and the axial direction of the projectile is about 34 °~41 °, indicating that the fracture mode at the impact end is mainly compression shear failure; It is concluded that the formation of middle and bottom fragments is due to the joint action of tension and shear; As the axial path continues to increase and the axial pressure continues to decrease, the jacket can no longer break. The size distribution of jacket breakage during target penetration is shown in the figure 11.

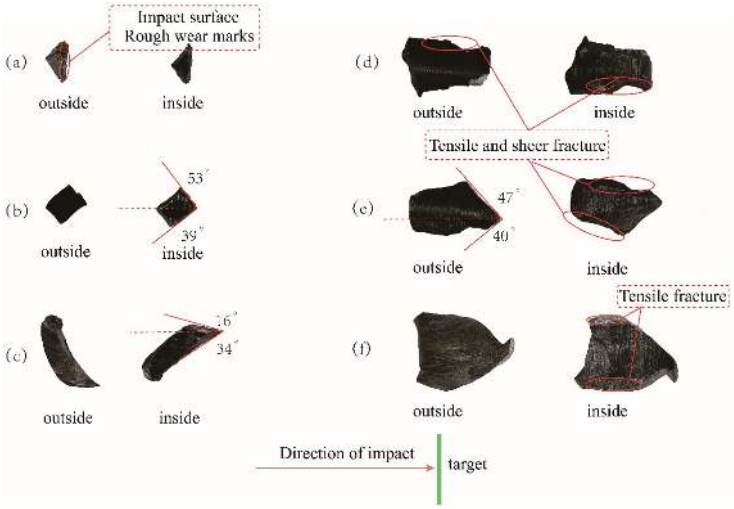


**Fig.10** Fragment morphology analysis

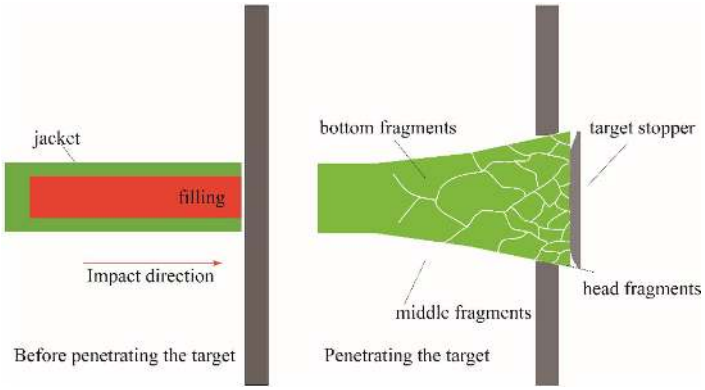


**Fig.11** Distribution of jacket fragmengs size under impact pressure

### 3.5 Analysis of aftereffect target fragment distribution

Figure 12 shows the damage of # 3, # 6 and # 8 PELE jacket fragments to the aftereffect target. Observe the distribution of jacket fragments behind the main target, which is mainly caused by the perforation of the whole penetrator and the bottom support. There are many small holes that not penetrated are speculated to be caused by the detritus of the filling, so its are not included in the number of upper target fragment; The number of fragments on the upper target in test#3 is 15, and the maximum distribution radius is 180mm; The number of upper target fragments in test #6 is 18, and the maximum distribution radius is 225mm; The number of upper target fragments in test#8 is 8, and the maximum distribution radius is 200mm. Since the fragment radial velocity is linear with the fragment distribution radius or the fragment dispersion angle, the fragment distribution radius can reflect the fragment radial velocity, and the farther away from the target center, the greater the fragment radial velocity.

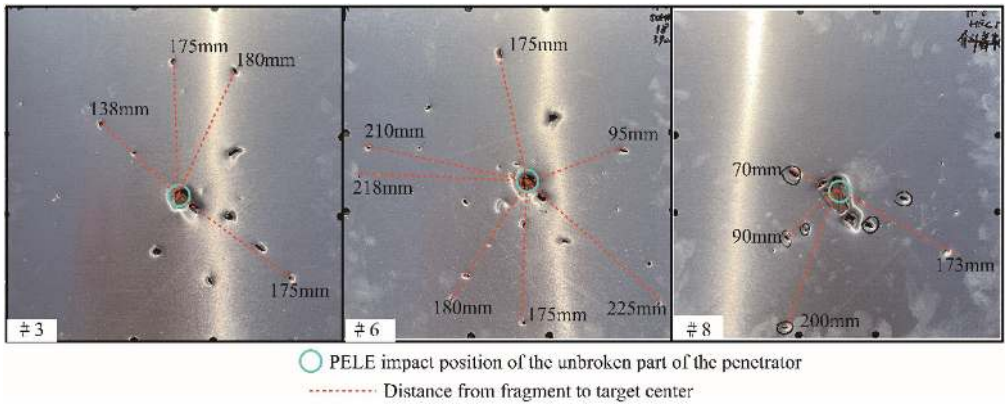


**Fig.12** 2A12 aluminum target fragment distribution

### 3.6 Degree of fragmentation and radial velocity analysis

Verreault (2015) supposed that after the penetrator head penetrates the target , the radial constraint of the target on the jacket behind the target disappears. At this time, the stopper still compresses the axial stress in the filling, which is converted into the radial stress due to Poisson effect, and acts on the inner wall of the jacket. From the moment when the penetrator head penetrates the target , the jacket and filling begin to break. Within a period of time when the bullet core head penetrates the target plate, the shell is in a process of axial motion and breaking at the same time, until the shell is broken after moving a certain distance behind the target, No new fragments will be produced. Analyzed the reason for the phenomenon in this paper. With the same thickness of the target, the time for the penetrator head to penetrate the target and the time for the stress wave to reflect on the front and back of the target are the same; Assuming that the thickness of the target is thick enough to load the axial stress of the filling to the whole distance, when the filling generates radial stress on the jacket, the higher the fracture strain, the better the toughness of the jacket. The jacket with small fracture strain completes the most ideal crushing earlier than the jacket with large fracture strain (it is completely broken except for the bullet bottom). However, the jacket with large fracture strain only has deformation on the head and partial fracture on the head due to the thin thickness of the target, It takes a short time for the bullet head to penetrate the target plate, and the

time for the shock wave to radiate back and forth on the front and back of the target plate is also short, which causes the unloading wave to arrive in advance and unload the bullet core. The bullet core cannot continue to compress according to the original compression strength, and the compression path is limited. Therefore, the shell with large fracture strain only has head bending fracture, and the reason for the head fracture may not be that the radial strain of the shell reaches the corresponding fracture strain, It is a complex fracture mode under the combined action of bullet core and target plate, so the radial velocity cannot be judged by the radial stress of bullet core to shell.

At the moment of penetrator impact on the target, the pressure at the contact position between the penetrator and the target can be calculated by equation (1) (Chun, 2020a). At the moment of impact , the pressure between the filling and the target is:

$$P_f = v_0 \frac{\rho_f U_f \rho_t U_t}{\rho_f U_f + \rho_t U_t} \tag{1}$$

In the equation, $\rho$ is the density and $U$ is the shock wave velocity. For one-dimensional strain problems, it can be expressed by the plastic wave velocity in the material. The subscripts $f$ and $t$ represent the filling and target respectively, $v_0$ is the impact velocity of the penetrator. The pressure between the filling and the target can be regarded as the axial stress of the penetrator, namely, $P_f = \sigma_x$ .

The radial stress is:

$$\sigma_y = \frac{v_f}{\left(1-v_f\right)+\frac{E_f}{E_j}\left(1-v_j\right)}\sigma_x \tag{2}$$

When the radial expansion of the jacket is less than the radial expansion of the filling, the radial stress related to jacket breakage occurs. The radial expansion of the filling is obtained from the generalized Hooke's law, where the relationship between the strain and the radial stress and the axial stress is as follows:

$$\varepsilon_j = \frac{\left(1-v_j\right)\sigma_y}{E_j} \tag{3}$$

The relationship between radial strain and radial stress of jacket is

$$\varepsilon_j = \frac{\left(1-v_j\right)\sigma_y}{E_j} \tag{4}$$

The critical fracture strain of penetrator jacket under different target velocity is calculated as shown in Figure 13. It can be seen that the critical fracture strain required for the jacket to break its own material increases with the increase of target velocity (Chun, 2020b); Compared with the measured fracture strain in the test, the jacket of HRC30 is not broken because the fracture strain is greater than the critical fracture strain at the target velocity; The fracture strain of the jacket of HRC50 is less than the critical fracture strain at the target velocity, so the jacket plays a fragmentation effect.

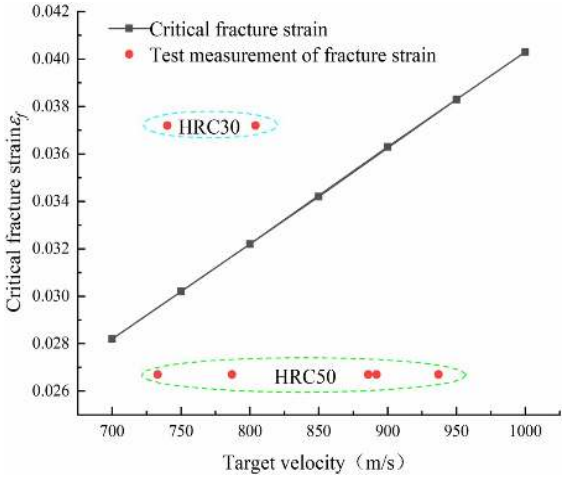


**Fig.13** Relationship between penetrator fracture strain and critical fracture strain at different target velocities

## 4 CONCLUSION

(1) After quenching and tempering, the hardness of 30CrMnSiA increases, and the corresponding fracture strain decreases. Under the tensile action, the plasticity decreases, and the brittleness increases. Under the axial and radial loads, shear damage easily occurs;

(2) The HRC50 jacket PELE penetrator has a fragmentation effect after penetrating the target plate, and the maximum fragment distrbtion radius is 25 times of the projectile radius, while the jacket radial strain of the HRC30 jacket PELE after penetrating the target plate does not reach the fracture strain and cannot produce a fragmentation effect;

(3) The main fracture modes of HRC50 jacket are shear failure and shear tensile failure. The fragment size increases gradually from head to tail;

(4) Fracture strain is one of the factors controlling the failure and fragmentation of metals. Under the same impact pressure, the smaller the fracture strain is, the easier the metal is to be broken; And the fragmentation effect increases with the increase of target velocity; The higher the impact velocity, the smaller the critical fracture strain of the jacket.

## Acknowledgement

The author(s) disclose the receipt of the following financial support for the research, authorship, and/or publication of this article: The project was supported by Supported by Supported by National Natural Science Foundation of China(12202207).

**Author's Contributions:** Conceptualization, Yuheng Liu and Lizhi Xu; Methodology, Yuheng Liu, Lizhi Xu, Heling Zheng, Meng Xu, Wenzheng Lv; Writing - original draft, Yuheng Liu; Writing - review & editing, Yuheng Liu; Funding acquisition, Lizhi Xu; Resources, Lizhi Xu, Zhonghua Du.

**Editor**: Marcílio Alves

## References

Zhu Jiansheng, Fan Zhi, Du Zhonghua Effect of shell material on PELE effect [J] Weapon Material Science and Engineering, 2010, 06:14-16.

Chen Pu Research on PELE projectile fragmentation and lateral reaming effect [D] Changsha National University of Defense Science and Technology, 2014.

Fan Zijian Research on penetration and fragmentation mechanism of projectile enhanced by lateral effect [D] National University of Defense Science and Technology, 2016.

Cheng Chun, DU Zhonghua, CHEN Xi, et al. Numerical Simulation for Impact Fragmentation of Jacket Grooved PELE [J]. Journal of Ballistics, 2019, 31(3): 92-6.

Verreault J. Analytical and numerical description of the PELE fragmentation upon impact with thin target plates[J]. International Journal of Impact Engineering, 2015, 76(76):196-206.

Chun Cheng, Lizhi Xu, Zhonghua Du et al. Perforation Characteristics of Metal Target plate subjected to PELE[J]. Latin American Journal of Solids and Structures, 2020a, 17(4):1-16.

Chun Cheng, Xi Chen, Zhonghua Du et al. Fragmentation Characteristics and Damage capacity Radial Layered PELE[J]. Latin American Journal of Solids and Structures. 2020b, 17(8): 1-14.